ORIGINAL PAPER

Synthesis and electrochemical properties of $Ca_{0.9}La_{0.1}WO_{4+\delta}$ electrolyte for solid oxide fuel cells

Jihai Cheng · Changan Tian · Difang Zhao

Abstract $Ca_{0.9}La_{0.1}WO_{4+\delta}$ powder was prepared by gel auto-ignition process. According to X-ray diffraction analysis, the resulted $Ca_{0.9}La_{0.1}WO_{4+\delta}$ solid solution has tetragonal scheelite structure. Results of electrochemical testing reveal that the performances of La-doped calcium tungstate are superior to that of pure $CaWO_4$, a conductivity of 5.28×10^{-3} S cm^{-1} at 800 °C could be obtained in the $Ca_{0.9}La_{0.1}WO_{4+\delta}$ compound sintered at 1,200 °C. The electrical conductivity as a function of oxygen partial pressure and also the electromotive force of oxygen concentration cell are measured to prove the mainly ionic conductivity of the investigated material.

Keywords Solid oxide fuel cells · Electrolyte · Electrochemical property · Scheelite structure

Introduction

Solid oxide fuel cells (SOFCs) are efficient and clean energy devices. The lowering of the operating temperature below 700 °C has been one of the main issues in SOFCs development [1–3]. Ionically conducting solids, especially oxide ion conductors, have potential use for electrolyte materials of SOFCs [4]. A lot of ionic conductors have been found in various systems. Among these materials, yttria-stabilized zirconia (YSZ) and CeO_2-based fluorite-type oxides are the most popular conductors. However, their high operating temperature results in both high costs and system degradation at the interface between cell components [5, 6]. In recent years, some new materials that proposed to substitute for the YSZ types of electrolytes have been reported as electrolytes for SOFCs.

Currently, a new ionic conductor based on the scheelite-type oxide has attracted much interest because of its potential application as electrolyte material in SOFCs [7, 8]. This scheelite structure can be easily doped with rare-earth ions, and the doped oxide can be used as an important functional material. Typical examples of scheelite-type oxides are $CaWO_4$, $SrWO_4$, $PbWO_4$, and $BaWO_4$. After doping, these scheelite-type oxides exhibit a high oxide ion conduction in the intermediate temperature range, e.g., $Pb_{0.9}Sm_{0.1}WO_{4+\delta}$ shows a conductivity of 2×10^{-2} S cm^{-1} at 800 °C [7], which is comparable to that of YSZ electrolytes (3.6×10^{-2} S cm^{-1} at 800 °C). A wide variety of properties for compounds with the scheelite structure, especially electrical conduction of various substituted scheelite-type samples, have been explored [9–11].

In the present study, the $Ca_{0.9}La_{0.1}WO_{4+\delta}$ powder was prepared by the auto-ignition process. Its phase information and sinterability were investigated. Additionally, the electrical properties of $Ca_{0.9}La_{0.1}WO_{4+\delta}$ sintered samples were characterized to estimate if they could serve as an alternative electrolyte for SOFCs.

J. Cheng · C. Tian · D. Zhao
Department of Chemistry and Materials Engineering,
Hefei University,
Hefei 230022, China

J. Cheng (✉)
Key Lab of Powder and Energy Sources Materials,
Hefei University,
Hefei 230022, China
e-mail: cjh@hfuu.edu.cn

Experimental

The synthesis of $Ca_{0.9}La_{0.1}WO_{4+\delta}$ was performed by the gel auto-ignition route. Stoichiometric amounts of Ca

$(NO_3)_2 \cdot 4H_2O$, $La(NO_3)_3 \cdot 6H_2O$, $(NH_4)_6H_2W_{12}O_{40}$, and citric acid (AR grade, Sinopharm Chemical Reagent Co. Ltd., China) were used as starting materials. These reactants were dissolved into deionized water and mixed together to form a gel by heating at about 80 °C; the wet gel was further heated to about 120 °C for 24 h to remove water. The dried gel was baked in an oven at 600 °C, where the combustion reaction took place within a few seconds to form the precursor. The powder was prepared by calcining the precursor at 900 °C for 2 h. The powder was pressed into pellets of 10 mm in diameter and 1–2 mm in thickness under the pressure of 200 MPa. Finally, the pellets were sintered at different temperatures (1,100–1,250 °C) for 4 h.

Differential thermal analysis (DTA) was performed in air from 50 to 700 °C at 10 °C min^{-1}. Phase formation of the calcined oxide powder was determined by X-ray diffraction (XRD: Model D/max-gB, Rigaku, Japan) analysis with the CuK$_\alpha$ line (λ=0.15406 nm) at angles ranging from 20° to 60°. For conductivity measurements, silver paste was painted onto both sides of the pellet samples and fired at 700 °C for 1 h to form Ag electrodes. The measurement of AC impedance was performed in air with an electrochemical workstation, CHI660B (Shanghai Chen Hua Instrument Co. Ltd., China). The frequency varied from 0.1 Hz to 100 kHz. Measurement of the data was conducted in the temperature range of 500–800 °C at an interval of 50 °C. The conductivity at each temperature was obtained after stabilizing the specimens for 30 min. For the oxygen concentration cell measurements, we used the method which has been reported by Norby et al. [12].

Results and discussions

DTA analysis

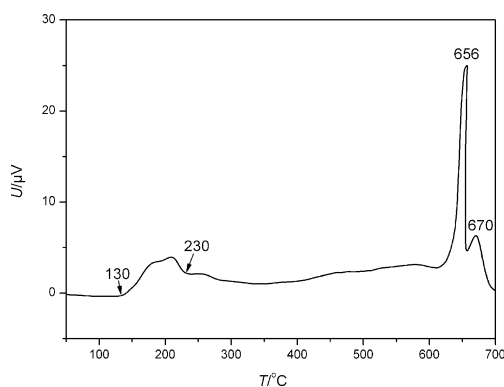The DTA of the dried gel was performed in order to study the decomposition and crystallization of the precursor. The

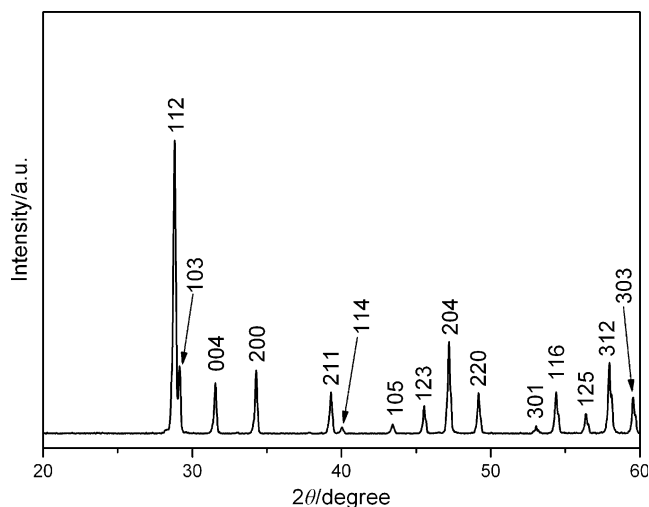**Fig. 1** DTA curve of $Ca_{0.9}La_{0.1}WO_{4+\delta}$ from 50 to 700 °C in air

Fig. 2 X-ray diffraction pattern of $Ca_{0.9}La_{0.1}WO_{4+\delta}$ calcined powder

DTA plot for the $Ca_{0.9}La_{0.1}WO_{4+\delta}$ sample is shown in Fig. 1. Three exothermic peaks are observed: at 130–230, 656, and 670 °C, respectively. The exothermic peaks at 130–230 °C corresponded to the initial decomposition of citric acid and the precursor in the dried gel. The exothermic peak appearing at 656 and 670 °C indicated the decomposition/oxidation reactions. They are attributed to the pyrolysis of nitrates in the precursor and the formation of the nucleus of the crystal and crystallization of $Ca_{0.9}La_{0.1}WO_{4+\delta}$. The observations of these phenomena support the conclusion based on DTA analysis that $Ca_{0.9}La_{0.1}WO_{4+\delta}$ precursors begin to decompose from near 130 °C and phase formation proceeds subsequently from near 650 to 700 °C.
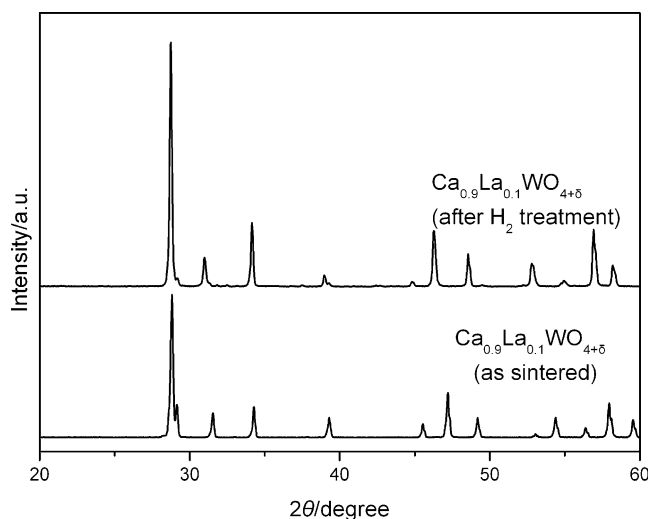
Fig. 3 X-ray diffraction patterns of $Ca_{0.9}La_{0.1}WO_{4+\delta}$ sintered samples before and after exposing to H_2 atm at 900 °C for 2 h
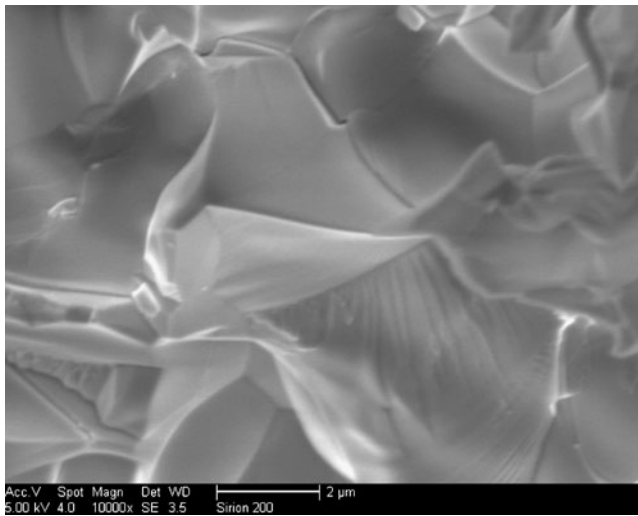
Fig. 4 Cross-section of $Ca_{0.9}La_{0.1}WO_{4+\delta}$ electrolyte sintered at 1,200 °C for 4 h

peaks matched well with the PDF file no. 77-2237. No additional diffraction peaks were found, indicating that the substitution of the La^{3+} ion at the Ca^{2+} site had occurred and formed a solid solution with the general formula of $Ca_{0.9}La_{0.1}WO_{4+\delta}$ composed of a single tetragonal scheelite phase.

In order to verify the stability in such an atmosphere where the SOFCs operate, especially in a reducing atmosphere, the sintered samples were exposed to H_2 atm at 900 °C for 2 h and phase composition was then investigated. Figure 3 shows the X-ray diffraction patterns of the surface of the sintered $Ca_{0.9}La_{0.1}WO_{4+\delta}$ before and after exposing. The diffraction pattern of the specimen after H_2 treatment was the same as that of untreated sample. That is to say, scheelite-type $Ca_{0.9}La_{0.1}WO_{4+\delta}$ material might have satisfactory chemical stability under reducing atmospheres and meets the requirement of the electrolyte in SOFCs.

Phase information

The XRD patterns of the $Ca_{0.9}La_{0.1}WO_{4+\delta}$ powder calcined at 900 °C for 2 h are illustrated in Fig. 2. All diffraction

Sintering behavior

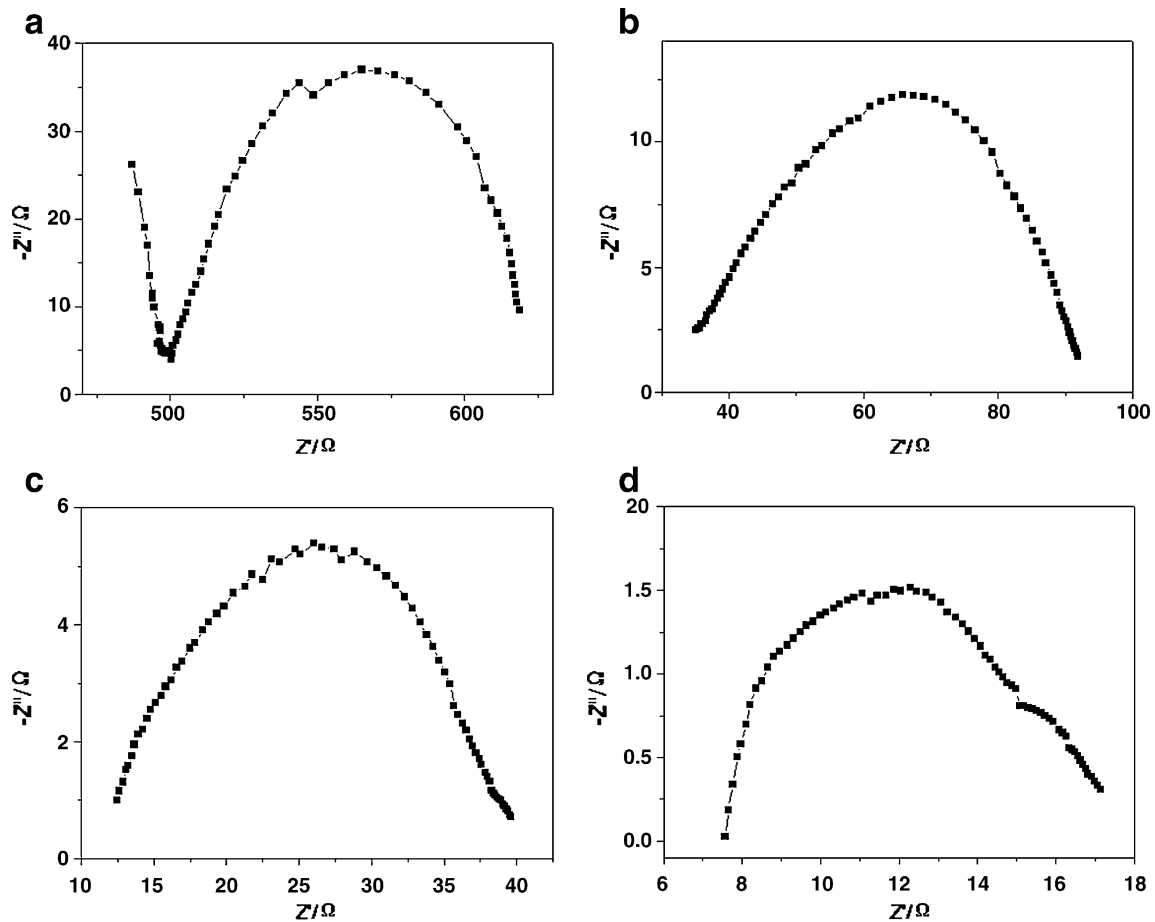The relative density of the sintered ceramic samples was measured using the standard Archimedes method and

Fig. 5 Impedance spectra of $Ca_{0.9}La_{0.1}WO_{4+\delta}$ tested at: (**a**) 500 °C, (**b**) 600 °C, (**c**) 700 °C, and (**d**) 800 °C
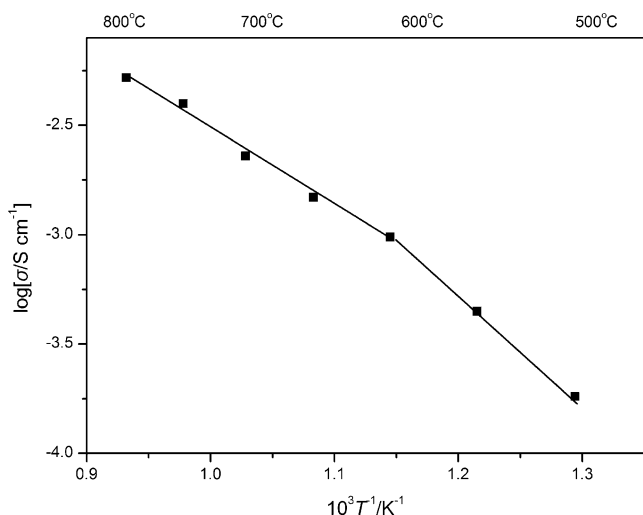
Fig. 6 Arrhenius plot showing the total conductivity of $Ca_{0.9}La_{0.1}WO_{4+\delta}$

Fig. 8 Electrical conductivity of $Ca_{0.9}La_{0.1}WO_{4+\delta}$ at 800 °C as a function of oxygen partial pressure

94.5% of the theoretical density was obtained in the $Ca_{0.9}La_{0.1}WO_{4+\delta}$ sample after being sintered at 1,200 °C for 4 h. This temperature is considerably lower than that of other fluorite or perovskite type electrolytes [13–15].

Figure 4 exhibits a cross-sectional view of the $Ca_{0.9}La_{0.1}WO_{4+\delta}$ electrolyte sintered at 1,200 °C for 4 h. The electrolyte pellet is quite dense and uniform; the cross-sectional view is void of any obvious pores and cracks, which indicates good sintering.

Electrical conductivity

The electrical conductivity of sintered ceramics was measured by AC impedance method. Figure 5 shows typical impedance plots for $Ca_{0.9}La_{0.1}WO_{4+\delta}$-sintered

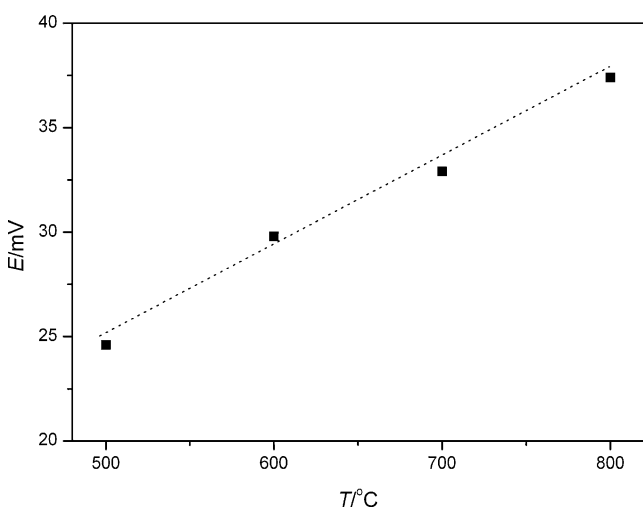pellets measured in air at various temperatures. A single semicircle was observed and the low frequency intercept is measured for evaluation of the conductivity data. The impedance spectral data were fitted with a suitable equivalent circuit of the Zsimpwin software to distinguish the bulk resistance and grain-boundary resistance, and calculate the conductivities. Representative Arrhenius plot of conductivity measured in air is shown in Fig. 6. Higher conductivity is observed after La doping. For pure $CaWO_4$, the conductivity is lower than 10^{-5} S cm^{-1} at 900 °C [7]. The conductivity of $Ca_{0.9}La_{0.1}WO_{4+\delta}$ sintered at 1,200 °C for 4 h in air reached 5.28×10^{-3} S cm^{-1} at 800 °C. To our opinion, the partial substitution of Ca with La in scheelite structure might cause two opposite effects. The ordering of the oxygen vacancy might be suppressed, which led to the decrease in activation energy of conduction and an increase in ionic conductivity [16]. Additionally, the deviation of the

Fig. 7 Temperature dependence of the EMF of the cell: O$_2$ (0.21 atm), Ag|$Ca_{0.9}La_{0.1}WO_{4+\delta}$|Ag, O$_2$ (1 atm). The *dashed line* denotes the theoretical EMF obtained by the Nernst equation
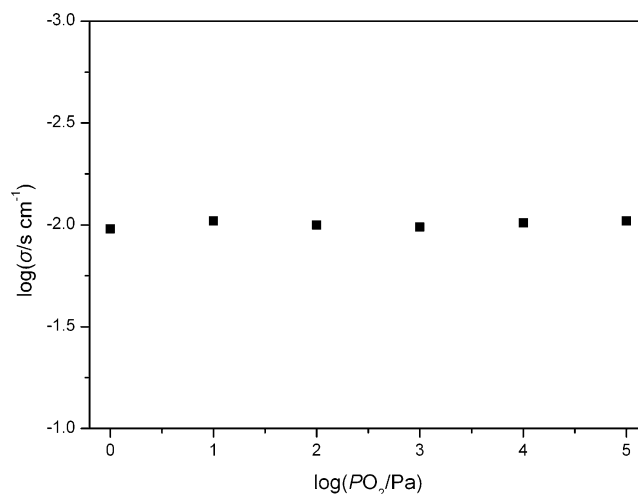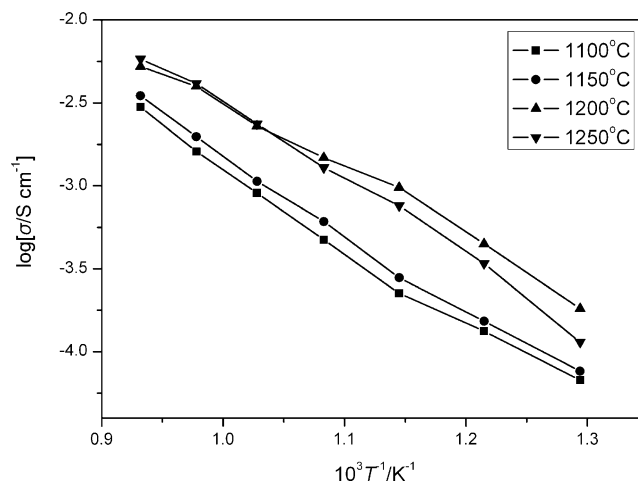

Fig. 9 Dependencies of the conductivity on temperature for $Ca_{0.9}La_{0.1}WO_{4+\delta}$ ceramics sintered at different temperatures

lattice parameter from that of pure $CaWO_4$ was positive, which led to the increase in the activation energy of conduction and the decrease in ionic conductivity. Therefore, the electrolyte with the greater ionic conductivity must contain an appropriate dopant concentration.

The activation energies for $Ca_{0.9}La_{0.1}WO_{4+\delta}$ samples can be obtained from Arrhenius plot (Fig. 6). They were calculated for two temperature regions: above 600 °C and below 600 °C. These two different values show contribution of the two different types of charge carriers [16]. The conductivity at the high temperature region (>600 °C) is expressed by

$$\sigma T = A_1 \exp\left(-\frac{E_1}{\kappa T}\right) \tag{1}$$

with

$$E_1 = \frac{1}{2}h_F + h_m \tag{2}$$

where h_F is the energy of formation of Frenkel defects and h_m is the migration energy of the mobile species. At low temperature (<600 °C), the conductivity being determined by the frozen-in defects, is given by

$$\sigma T = A_2 \exp\left(-\frac{E_2}{\kappa T}\right) \tag{3}$$

where

$$E_2 = h_m \tag{4}$$

Should the same carrier be mobile in the two temperature regions, the Frenkel defect formation energy h_F can be computed from Eqs. 2 and 4 as

$$h_F = 2(E_1 - E_2) \tag{5}$$

The activation energies E_1 and E_2, calculated from the two slopes are presented along with Frenkel defect formation energy of each of the different crystal compositions. It is essentially implied that the activation enthalpy of the low temperature region is lower than the one of the high temperature conductivity [4, 16, 17]. The activation energies of the $Ca_{0.9}La_{0.1}WO_{4+\delta}$ sample in the two temperature regions are 0.46 and 0.67 eV, respectively.

In order to check the charge carriers in $Ca_{0.9}La_{0.1}WO_{4+\delta}$, the following oxygen gas concentration cells were constructed using sample pellets as electrolytes, and the cell electromotive forces (EMFs) were measured:

$$-O_2(0.21atm), Ag \mid Ca_{0.9}La_{0.1}WO_{4+\delta} \mid Ag, O_2(1\,atm) +. \tag{6}$$

Figure 7 shows EMFs measured by oxygen gas concentration cells constructed using samples as the electrolytes, air

and 1 atm oxygen gas as the anode and cathode gas, respectively. Measured EMFs for $Ca_{0.9}La_{0.1}WO_{4+\delta}$ showed good coincidence with the value of the theoretical EMF for oxygen concentration cell calculated (E) from the Nernst equation, indicating that the ionic transport number of this compound was almost unity. In Fig. 8, electrical conductivity of $Ca_{0.9}La_{0.1}WO_{4+\delta}$ is shown as a function of oxygen partial pressure. As seen in Fig. 8, the conductivity does not change with oxygen partial pressure, which indicated that the main charge carriers are oxide ions.

In order to investigate the effect of sintering temperature on the properties of $Ca_{0.9}La_{0.1}WO_{4+\delta}$, a series of sintering conditions were studied. The electrical conductivity (Fig. 9) increased as the sintering temperature increased and reached a maximum value (for 800 °C) of 5.28×10^{-3} S cm^{-1} when sintering temperature was 1,200 °C. However, when the sintering temperature exceeded 1,200 °C, the conductivity is rather similar or less than for sintering temperature of 1,200 °C. The reason may be that loss of the lattice oxygen in this system at high temperatures caused the decrease in electrical conductivity due to the reduction of charge carrier concentration [18].

Conclusions

The gel auto-ignition process was used to synthesize scheelite-type $Ca_{0.9}La_{0.1}WO_{4+\delta}$ electrolyte material. The phase formation, sintering behavior, and electrochemical properties of this compound were investigated. Results indicated that, when doped with trivalent La^{3+} cations, scheelite-type $Ca_{0.9}La_{0.1}WO_{4+\delta}$ samples show show good sinterability and relatively high total conductivity. The oxygen gas concentration cells testing results show that the main ionic charge carriers were oxide ions. Considering the level of conductivity and the stability in reducing atmospheres at high temperature, the application of these materials in SOFCs electrolyte could be considered.

References

1. Hansen KK, Hansen KV, Mogensen M (2010) J Solid State Electrochem 14:2107–2112
2. Serincana MF, Pasaogullaria U, Sammes NM (2009) J Power Sources 194:864–872
3. Moon H, Kim SD, Hyun SH, Kim HS (2008) Int J Hydrogen Energ 33:1758–1768

4. Esaka T, Tachibana R, Takai S (1996) Solid State Ionics 92:129–133

5. Lee D, Han JH, Chun Y, Song RH, Shin DR (2007) J Power Sources 166:35–40

6. Huang B, Zhu XJ, Hu WQ, Yu QC, Tu HY (2009) J Power Sources 186:29–36

7. Esaka T (2000) Solid State Ionics 136–137:1–9

8. Thangadurai V, Knittlmayer C, Weppner W (2004) Mater Sci Eng B 106:228–233

9. Cheng JH, Bao WT, Han CL, Cao WB (2010) J Power Sources 195:1849–1853

10. Tsipis EV, Munnings CN, Kharton VV, Skinner SJ, Frade JR (2006) Solid State Ionics 177:1015–1020

11. Maurera MAMA, Souza AG, Soledade LEB, Pontes FM, Longo E, Leite ER, Varela JA (2004) Mater Lett 58:727–732

12. Norby T, Kofstad P (1986) J Am Ceram Soc 69:780–783

13. Wang Q, Peng R, Xia C, Zhu W, Wang H (2008) Ceram Int 34:1773–1778

14. Zhong Z (2007) Solid State Ionics 178:213–220

15. Han M, Tang X, Yin H, Peng S (2007) J Power Sources 165:757–763

16. Arora SK, Godbole RS, Lakshminarayana D (1983) J Mater Sci 18:1359–1364

17. Cheng JH, Liu CF, Cao WB, Qi MX, Shao GQ (2001) Mater Res Bull 46:185–189

18. Zhao H, Teng D, Zhang X, Zhang C, Li X (2009) J Power Sources 186:305–310